Appl. Sci. Converg. Technol. 24(6): 268-272 (2015)
http://dx.doi.org/10.5757/ASCT.2015.24.6.268

Research Paper

Toward Charge Neutralization of CVD Graphene

Soo Min Kim[a] and Ki Kang Kim[b]*

[a]*Institute of Advanced Composite Materials, Korea Institute of Science and Technology (KIST), San101 Eunha-Ri, Bongdong-Eup, Wanju-Gun, Jeollabuk-Do 565-902, Korea*

[b]*Department of Energy and Materials Engineering, Dongguk University-Seoul, Seoul 410-820, Korea*

Received October 23, 2015; revised November 6, 2015; accepted November 6, 2015

Abstract We report the systematic study to reduce extrinsic doping in graphene grown by chemical vapor deposition (CVD). To investigate the effect of crystallinity of graphene on the extent of the extrinsic doping, graphene samples with different levels of crystal quality: poly-crystalline and single-crystalline graphene (PCG and SCG), are employed. The graphene suspended in air is almost undoped regardless of its crystallinity, whereas graphene placed on an SiO_2/Si substrate is spontaneously p-doped. The extent of p-doping from the SiO_2 substrate in SCG is slightly lower than that in PCG, implying that the defects in graphene play roles in charge transfer. However, after annealing treatment, both PCG and SCG are heavily p-doped due to increased interaction with the underlying substrate. Extrinsic doping dramatically decreases after annealing treatment when PCG and SCG are placed on the top of hexagonal boron nitride (h-BN) substrate, confirming that h-BN is the ideal substrate for reducing extrinsic doping in CVD graphene.

Keywords: graphene, doping, chemical vapor deposition, single crystalline, hexagonal boron nitride

I. Introduction

Graphene has been highlighted due to its unique physical and chemical properties such as massless Dirac behavior, high carrier mobility, and superb mechanical strength; utilization of these properties has led to potential applications such as transparent conducting electrodes for flexible electronics, radio-frequency devices, and atomic membranes [1-7]. To realize such applications, control of the doping level in graphene is one of several important issues. Essentially, to maximize the performance of electronic devices [8,9], maintaining of the charge neutrality in graphene is highly necessary. Since all the carbon atoms in monolayer graphene are exposed to air and are in contact with the underlying substrate, the doping level is strongly affected by the environmental conditions. For instance, when graphene is placed on an SiO_2/Si substrate in air, it typically shows p-type behavior due to charge transfer from the dipole adsorbates and diatomic oxygen in the SiO_2 substrate [10].

To reduce extrinsic doping from the environment, hydrophobic and hexagonal boron nitride (h-BN) substrates have been suggested. The hydrophobic substrate, prepared by coating with fluoropolymer or hexamethyldisilazane on SiO_2/Si, helps in the reduction of extrinsic doping from the substrate and from water in air [10,11]. The h-BN substrate, posing free of dangling bonds on the surface and atomically flat surface effectively leads to charge neutrality in graphene [3].

Initially, graphene was prepared by using the mechanical exfoliation method, producing single-crystalline graphene (SCG). The size was limited to a few micrometers [12]. Therefore, this material could not be utilized for large-area applications. More recently, large-area graphene has been realized using the chemical vapor deposition method (CVD-graphene) on Cu foil [13]; however, this process produces both single-crystalline graphene (SCG) and poly-crystalline graphene (PCG) depending on the growth conditions [13,14]. Two main differences between SCG and PCG should be mentioned. First, the crystallinity of SCG is higher than that of PCG due to imperfections of graphene film caused by grain boundaries or defects (structural defects) [13]. Second, CVD-graphene grown on Cu foil is transferred onto an arbitrary substrate using the wet etching process. During the wet etching process, the structural defects are easily functionalized, inducing the formation of dipolar adsorbates such as water or oxygen [15,16]. These structural defects might affect the doping level of graphene. However, the effect of the crystallinity of graphene on the extrinsic charge doping has not been studied so far.

Here, we systemically study how to reduce extrinsic doping of CVD-graphene. To study the effect of the crystallinity of graphene, two kinds of graphene were synthesized: PCG and SCG. In addition, to examine the

*Corresponding author
E-mail: kkkim@dongguk.edu

effect of the substrate, CVD-graphene is transferred to various kinds of substrate, including TEM grids for suspended graphene, hexagonal boron nitride (hBN), 300 nm SiO_2/Si, and, octadecyltrichlorosilane (OTS)-treated SiO_2/Si substrate After graphene is transferred to the various substrates, poly (methyl methacrylate) (PMMA), used as a supporting layer during the transfer process, is removed by acetone. To remove the dipole adsorbates and PMMA residues on graphene, annealing treatment under a forming gas is carried out. Raman spectroscopy is employed to track the extrinsic doping in graphene. Even after heat treatment, suspended graphene presents a low doping level regardless of its crystallinity, whereas graphene is heavily p-doped on an SiO_2/Si substrate. Extrinsic doping is dramatically reduced when CVD-graphene is placed on OTS or h-BN substrates. In addition, PCG shows slightly higher p-doping than SCG does on any substrate, implying that structural defects play a role in extrinsic doping.

II. Experimental

Graphene was synthesized by low pressure CVD on Cu foil (25 μm, Alfa Aesar) as a catalytic substrate. Prior to graphene growth, the Cu foil was annealed at 1035ºC for 30 min under hydrogen atmosphere at a rate of 10 sccm to yield a smooth Cu surface and increase the Cu grain size. To grow PCG and SCG, different Cu geometries, flat Cu foil for PCG and Cu foil enclosure for SCG, as detailed in previous works, were applied [13, <XREF>14]. While PCG was grown by flowing 5 and 10 sccm of methane and hydrogen, respectively, at 1035ºC for 30 min, SCG was grown by flowing 1 and 10 sccm of methane and hydrogen, respectively. After the growth process, the temperature was cooled quickly by opening the CVD chamber. Graphene was transferred by conventional PMMA method. PMMA (4.5% in anisole, Microchem) as a supporting layer was spun at 2,500 rpm for 1 min on graphene/Cu. To understand the effect of Cu etchant on the extrinsic doping, two different etchants, an $FeCl_3$-based etchant (CE-100, Transene) and an ammonium persulfate (APS-100, Transene)-based etchant were used. After etching of the Cu foil, the resultant film was transferred onto different substrates: a TEM grid (2.5 μm hole, Tel Pella) for suspended graphene, hexagonal boron nitride (h-BN), 300 nm SiO_2/Si, and octadecyltrichlorosilane (OTS, Sigma-Aldrich)-treated SiO_2/Si substrate. For the h-BN substrate, single crystalline hBN was mechanically exfoliated on the SiO_2/Si substrate [3]. For the OTS substrate, self-assembled monolayers were formed on freshly plasma-cleaned SiO_2 substrates in OTS solution (10 mM in toluene) overnight in a closed vial; seld-assembled monolayers were then rinsed in fresh toluene and were blown dry with nitrogen [17]. The PMMA layer on graphene was removed by rinsing with acetone. To further remove the PMMA residues and any dipole adsorbate on graphene, the graphene film was annealed at 350ºC for 5 hours under hydrogen and argon atmospheres at flow rates of 300 and 700 sccm, respectively. To analyze the extent of extrinsic doping, Raman spectroscopy (home-built Raman spectrometer with ~5 cm^{-1} resolution and a laser excitation at 2.33 eV) was employed. To observe the surface morphology of graphene on the substrate, optical microscopy (Carl-Zeiss, objective 100x) was used.

II. Results and Discussion

To understand the effect of crystallinity of CVD-graphene on extrinsic doping, two kinds of graphene: poly-crystalline CVD-graphene (PCG) and single-crystalline CVD-graphene (SCG), were employed. Prior to studying the effect of the substrate, the intrinsic doping level of the CVD graphene was investigated using suspended graphene. Suspended sample is very useful to study the intrinsic state of graphene, because substrate effects are excluded. Both PCG and SCG samples were transferred using the conventional PMMA method onto a TEM grid. After etching the copper foil with Cu etchants ($FeCl_3$-based etchant or ammonium persulfate (APS)-based etchant), the resultant film was placed on a TEM gird to make suspended graphene (Fig. 1(a)). To remove the PMMA layer and dipole adsorbates, acetone and annealing treatments were utilized. Raman spectroscopy is a very useful tool to characterize the defects, doping level, and strain in graphene [18]. Prominent Raman features consist of a D-band near 1366 cm^{-1} due to structural defects, a G-band near 1580 cm^{-1} due to E_g symmetry at the Ã point, and a 2D-band near 2700 cm^{-1} due to 2nd order double-resonant Raman scattering. Typically, the blue-shifts of the G-band and the 2D-band indicate p-type doping in graphene, whereas the blue-shift of G-band and the red-shift of the 2D-band indicate n-type doping [19]. Fig. 1(b) shows the Raman spectra of the samples prepared by different methods. To understand the effect of PMMA, a PMMA-coated SCG sample (SCG-$FeCl_3$-PMMA) was first analyzed. The G-band of SCG-$FeCl_3$-PMMA is located at 1590 cm^{-1}, indicating that graphene is p-doped by PMMA or dipole adsorbates. After removing PMMA, the G-band was found to be downshifted to 1585 cm^{-1}, indicating that PMMA is a p-type dopant for graphene [20]. To eliminate the dipole adsorbates or PMMA residues on graphene, the samples were further annealed under forming gas. The G-band of SCG (SCF-$FeCl_3$-Annealing) was found to be red-shifted to 1582 cm^{-1} compared to the case of the SCG-$FeCl_3$-Acetone sample, implying that the dipole adsorbates or PMMA residues also induced p-type doping on graphene. Moreover, the G-band of PCG (PCG-$FeCl_3$-Annealing) shows a sample position (1582 cm^{-1}) similar to those of the SCG samples. These results indicate that CVD-graphene exists in the intrinsic state regardless of

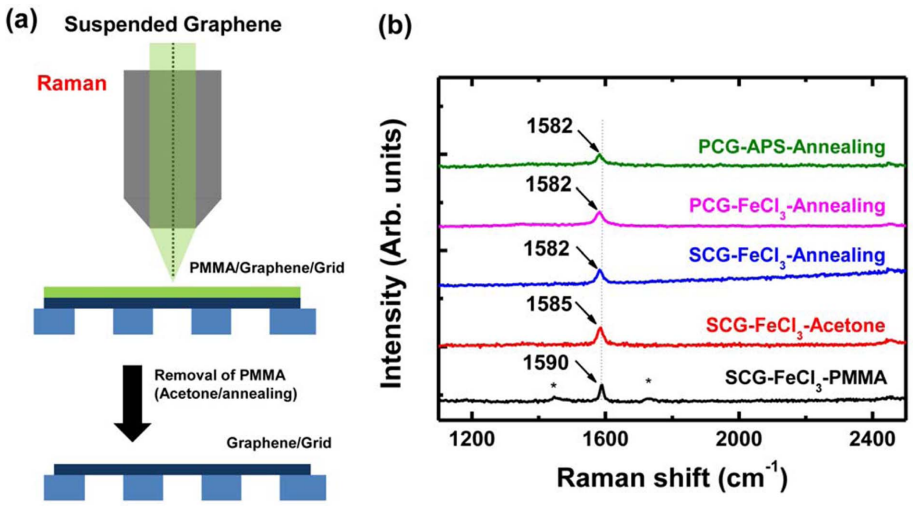

Figure 1. (a) Schematic diagram for Raman analysis of suspended graphene with different stages. (b) Raman spectra of suspended graphene: PMMA-coated graphene, acetone-treated graphene, thermal annealing-treated graphene. PCG and SCG denote poly-crystalline graphene and single-crystalline graphene, respectively. $FeCl_3$ and APS indicate two different Cu etchants, which were used for Cu etching during the transfer process.

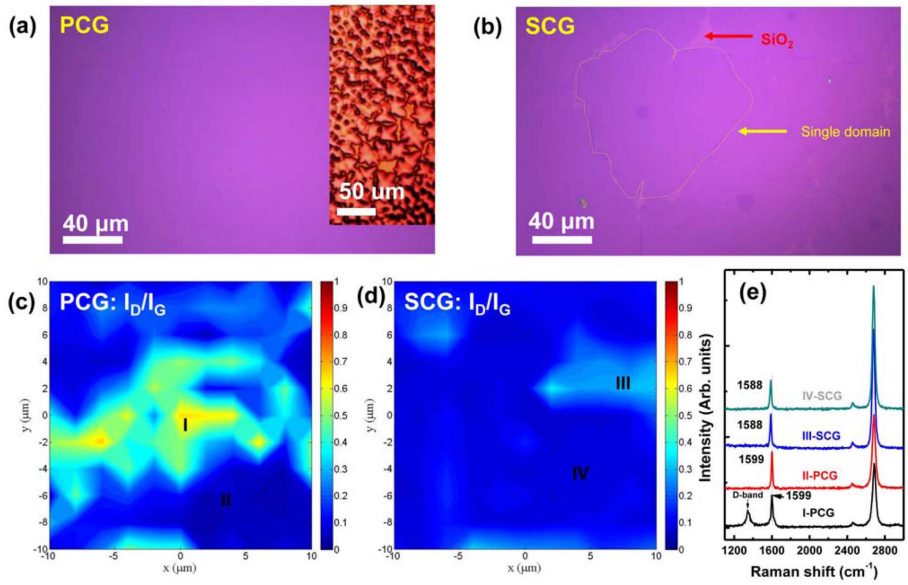

Figure 2. (a) and (b) Optical images of (a) PCG and (b) SCG. The inset in (a) shows an optical image of graphene on Cu foil before it is merged to form the continuous PCG-graphene film, proving that PCG has a polycrystalline structure with several graphene domains with sizes of less than 20×20 μm^2. The yellow dotted line in (b) shows the region of a single domain of graphene. (c) and (d) Raman mapping images of (c) PCG and (d) SCG for the intensity ratio of the D-band over the G-band. (e) Representative Raman spectra of the Roman numerals in (c) and (d).

its crystallinity. In addition, the G-band of the PCG sample prepared using APS etchant showed the same position (1582 cm^{-1}) as that of the PCG sample, indicating that the Cu etchant does not affect the doping level of graphene. According to previous work [19], the hole concentration of graphene can be deduced from the G-band position: 1582, 1585, and 1590 cm^{-1} correspond to hole concentrations of ~0×10^{12}, 3×10^{12}, and $7\times10^{12}/cm^2$, respectively. As a consequence, the doping level for suspended CVD-graphene becomes the intrinsic state and is not affected by the sample's crystallinity. Unfortunately, for real applications, CVD-graphene must be placed on a substrate; it cannot be used in air.

To understand the substrate effect, CVD-graphene was first transferred to the 300 nm SiO_2/Si substrate and the PMMA layer was removed using only acetone. Figs. 2(a) and (b) provide optical images of PCG and SCG on the 300 nm SiO_2/Si substrate. The PCG graphene is a highly continuous film. The inset of Fig. 2(a) shows an optical image of graphene on Cu foil before it is merged to form the continuous PCG-graphene film, proving that PCG has a polycrystalline structure with several graphene domains with sizes of less than 20×20 μm^2. Fig. 2(b) shows a single domain of a graphene flake, indicated by a yellow dotted line. To evaluate the crystallinity of both the PCG and SCG samples, Raman mapping was carried out. Figs. 2(c) and

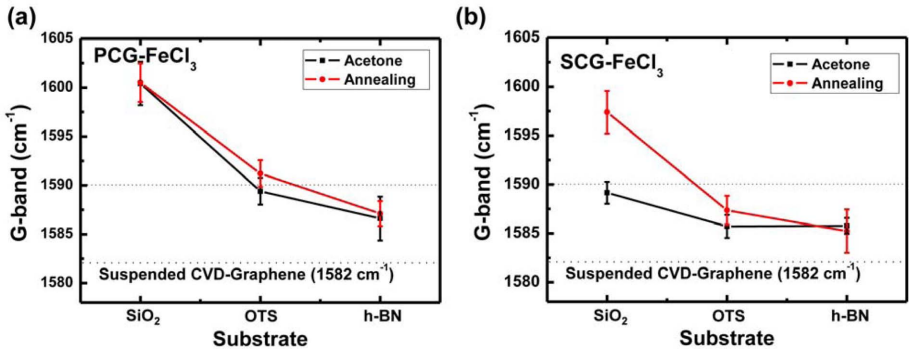

Figure 3. (a) and (b) G-band positions of (a) PCG and (b) SCG on three substrates, 300 nm SiO_2/Si, OTS, and h-BN, after acetone and thermal annealing treatments.

(d) show Raman mapping results for the intensity ratio of the D-band over the G-band for an area of 20×20 μm^2. The mapping image of PCG is not uniform, indicating that the crystallinity of PCG in this region fluctuated due to the polycrystalline structure. On the contrary, the Raman mapping image of SCG shows a quite uniform surface, except for certain regions. Fig. 2(e) shows the representative Raman spectra of the corresponding Roman numerals in Figs. 2(c) and (d). The intensity of the D-band/G-band in region I is higher than that in other regions, indicating that the crystallinity levels of those regions are lower. However, the G-band positions for the whole set of regions are the same at 1599 cm^{-1}. On the other hand, no prominent D-band for SCG was observed in regions III and IV, and the G-band position was located at 1588 cm^{-1}. These results indicate that both samples are p-doped more than suspended graphene is (G-band: 1585 cm^{-1}). Moreover, PCG is heavily p-doped compared to SCG. As a consequence, p-type doping in CVD-graphene can be said to have occurred due to three factors: dipole adsorbate/PMMA residues, SiO_2/Si substrate, and defects in graphene. First, the higher G-band position of SCG on the SiO_2/Si substrate (1588 cm^{-1}) compared to that of suspended SCG (1585 cm^{-1}) indicates that the SiO_2/Si substrate induces p-type doping. Second, because the structural defects in graphene easily trap the dipole adsorbates or PMMA residues, the heavier p-type doping in PCG (1599 cm^{-1}) compared to that in SCG (1588 cm^{-1}) suggests that the defects in PCG promote p-type doping [15].

The substrate effects were further studied with the various substrates, including the 300 nm SiO_2/Si, OTS-treated, and h-BN substrates. The OTS substrate is used for two reasons: first, graphene does not make contact with the SiO_2 substrate directly, reducing the interaction between graphene and SiO_2. Second, this substrate is known to be hydrophobic, and it can eliminate water trapping between graphene and the substrate, decreasing the p-doping on graphene [17]. The h-BN substrate was chosen due to its being free of dangling bonds on the surface and due to its atomically flat surface; this material is well known used as an ideal substrate for graphene [3]. After graphene was transferred onto these substrates, PMMA and dipole adsorbates were removed by acetone and thermal annealing treatments. Figs. 3(a) and (b) show the G-band position according to the various substrates after acetone and thermal annealing treatments, respectively. The G-band position of PCG-$FeCl_3$ on the SiO_2 substrate after both treatments is near 1600 cm^{-1}, implying that p-type doping in PCG has been saturated. Therefore, even after annealing, no further p-type doping occurred. On the other hand, the G-band position in SGC was at 1588 cm^{-1} and increased to 1598 cm^{-1} after acetone and thermal annealing. This result implies that the charge transfer between graphene and the substrate increased due to the increase of interaction between graphene and the SiO_2/Si substrate, which is in good agreement with the results of one previous report [21]. For the OTS substrate, while the G-band positions of PCG and SCG after acetone treatment were at 1589 and 1585 cm^{-1}, respectively, they were upshifted by 2 cm^{-1} after annealing treatment. This shows that the self-assembled OTS layer is thermally unstable due to its low melting point. However, this is a better substrate than the bare SiO_2/Si substrate because of the reduction of extrinsic doping by the SiO_2/Si substrate at room temperature. Lastly, the G-band positions of PCG and SCG on the h-BN substrate after both acetone and thermal annealing are near 1586 cm^{-1} and 1585 cm^{-1}, respectively. Even after annealing, the G-band position was unchanged due to the high thermal stability of h-BN. The lowest G-band positions for PCG and SCG after thermal annealing reached 1584 and 1583 cm^{-1}, respectively, which are close to the value of suspended graphene (1582 cm^{-1}). This implies that the doping level of CVD-graphene on h-BN has reached an almost intrinsic state. However, it is unclear why the G-band position of PCG on the h-BN and OTS substrates is always slightly higher than that on SCG except the G-band of suspended graphene. This may be attributed to structural defects in graphene interacting with the substrate.

IV. Conclusions

We systematically studied the effects of the crystallinity of CVD-graphene and the choice of substrates on extrinsic

doping in graphene. Suspended CVD-graphene is undoped regardless of its crystallinity. However, when CVD-graphene is placed on an SiO_2/Si substrate, PCG and SCG are p-doped by the substrate. The structural defects in PCG promote p-doping by introducing dipole adsorbate/PMMA residues on the graphene surface, meaning that PCG is always more p-doped than SCG is. Extrinsic doping is dramatically reduced when CVD-graphene is transferred onto an OTS or h-BN substrate. However, since the OTS substrate is unstable under thermal annealing, the h-BN substrate is a better choice than the OTS substrate.

Acknowledgments

S.M.K acknowledges the Korea Institute of Science and Technology (KIST) Institutional Program. K.K.K acknowledges support from the Basic Science Research Program through the National Research Foundation of Korea (NRF), funded by the Ministry of Science, ICT & Future Planning (2015R1C1A1A02037083).

References

[1] K. Novoselov, A. K. Geim, S. Morozov, D. Jiang, M. Katsnelson, I. Grigorieva, et al., Nature 438 197 (2005).
[2] A. K. Geim and K. S. Novoselov Nat. Mater. 6 183 (2007).
[3] C. Dean, A. Young, I. Meric, C. Lee, L. Wang, S. Sorgenfrei, et al. Nature Nanotech. 5 722 (2010).
[4] C. Lee, X. Wei, J. W. Kysar, and J. Hone Science, 321 385 (2008).
[5] S. Bae, H. Kim, Y. Lee, X. Xu, J.-S. Park, Y. Zheng, et al. Nat. Nanotech. 5 574 (2010).
[6] J. Moon, D. Curtis, M. Hu, D. Wong, C. McGuire, P. Campbell, et al. Electron Device Letters, IEEE 30 650 (2009).
[7] S. Garaj, W. Hubbard, A. Reina, J. Kong, D. Branton, and J. Golovchenko Nature 467 190 (2010).
[8] S. Morozov, K. Novoselov, M. Katsnelson, F. Schedin, D. Elias, J. Jaszczak, et al. Phys. Rev. Lett. 100 016602 (2008).
[9] J.-H. Chen, C. Jang, S. Xiao, M. Ishigami, and M. S. Fuhrer Nature Nanotech. 3 206 (2008).
[10] M. Lafkioti, B. Krauss, T. Lohmann, U. Zschieschang, H. Klauk, K. v. Klitzing, et al., Nano Lett. 10 1149 (2010).
[11] W. H. Lee, J. W. Suk, J. Lee, Y. Hao, J. Park, J. W. Yang, et al. ACS Nano 6 1284 (2012).
[12] K. Novoselov, D. Jiang, F. Schedin, T. Booth, V. Khotkevich, S. Morozov, et al. Proc. Natl. Acad. Sci. USA 102 10451 (2005).
[13] X. Li, W. Cai, J. An, S. Kim, J. Nah, D. Yang, et al. Science 324 1312 (2009).
[14] X. Li, C. W. Magnuson, A. Venugopal, R. M. Tromp, J. B. Hannon, E. M. Vogel, et al. J. Am. Chem. Soc. 133 2816 (2011).
[15] Y.-C. Lin, C.-C. Lu, C.-H. Yeh, C. Jin, K. Suenaga, and P.-W. Chiu Nano Lett. 12 414 (2011).
[16] J. Chan, A. Venugopal, A. Pirkle, S. McDonnell, D. Hinojos, C. W. Magnuson, et al. ACS Nano 6 3224 (2012).
[17] Q. H. Wang, Z. Jin, K. K. Kim, A. J. Hilmer, G. L. Paulus, C.-J. Shih, et al. Nat. Chem, 4 724 (2012).
[18] L. M. Malard, M. A. Pimenta, G. Dresselhaus, and M. S. Dresselhaus Phys. Rep. 473 51 (2009).
[19] A. Das, S. Pisana, B. Chakraborty, S. Piscanec, S. Saha, U. Waghmare, et al. Nat. Nanotech. 3 210 (2008).
[20] A. Pirkle, J. Chan, A. Venugopal, D. Hinojos, C. Magnuson, S. McDonnell, et al. Appl. Phys. Lett. 99 122108 (2011).
[21] Z. Cheng, Q. Zhou, C. Wang, Q. Li, C. Wang, and Y. Fang Nano Lett. 11 767 (2011).